

RSC Advances



This is an *Accepted Manuscript*, which has been through the Royal Society of Chemistry peer review process and has been accepted for publication.

Accepted Manuscripts are published online shortly after acceptance, before technical editing, formatting and proof reading. Using this free service, authors can make their results available to the community, in citable form, before we publish the edited article. This *Accepted Manuscript* will be replaced by the edited, formatted and paginated article as soon as this is available.

You can find more information about *Accepted Manuscripts* in the [Information for Authors](#).

Please note that technical editing may introduce minor changes to the text and/or graphics, which may alter content. The journal's standard [Terms & Conditions](#) and the [Ethical guidelines](#) still apply. In no event shall the Royal Society of Chemistry be held responsible for any errors or omissions in this *Accepted Manuscript* or any consequences arising from the use of any information it contains.

Studies on drastic improvement of photocatalytic degradation of acid orange -74 dye by TPPO capped CuO nanoparticles in tandem with suitable electron capturing agents

Aarti Sharma¹, Raj Kumar Dutta^{1,2*}

¹Centre of Nanotechnology, ²Department of Chemistry, Indian Institute of Technology Roorkee, Roorkee – 247667, India

***Corresponding Author: Email: duttafcy@iitr.ernet.in (R.K. Dutta)**

Abstract

Highly stable copper oxide (CuO) nanoparticles are synthesized by precipitation method and stabilized by *in situ* capping with triphenylphosphine oxide (TPPO). The as-synthesized CuO nanoparticles were characterized for average particle size (8 nm) by transmission electron micrograph (TEM); optical band gap of 2.29 eV by diffused reflectance spectroscopy and it revealed large BET surface area (105.82 m²/g). The poor sunlight induced photocatalytic activity towards degradation of acid orange 74 (an azo dye) by TPPO capped CuO nanoparticles was attributed to unfavorable electron capturing by molecular oxygen to produce reactive oxygen species, demonstrated from theoretical band structure calculation showing relative positioning of valence band (2.59 eV) and conduction band edges (0.29 eV) for TPPO capped CuO nanoparticles and those of redox potentials of O₂/O₂^{•-} (-0.2 eV) and H₂O/•OH (2.2 eV) in the NHE scale. Strikingly, TPPO capped CuO nanoparticles when mixed with 5 mM K₂S₂O₈ exhibited 99 % degradation of acid orange-74 in 180 min under sunlight exposure. Similar dye degradation efficiency was observed when CuO nanoparticles were mixed with H₂O₂ in reaction medium. The mechanism for drastic improvement in the dye degradation due to addition of K₂S₂O₈ or H₂O₂ has been explained on the basis of favorable redox couples of S₂O₈²⁻/SO₄^{•-} (2.01

eV) and $\text{H}_2\text{O}_2/\cdot\text{OH}$ (0.87 eV) which could accept photoexcited electrons from conduction band of CuO to produce reactive hydroxyl radical species. Using selective scavenger for reactive oxygen species, the generation of $\text{O}_2^{\cdot-}$ was ruled out and hydroxyl radicals were confirmed as the major reactive oxygen species for degradation of acid orange-74 dye. Ion chromatography studies of the aliquot left after sunlight induced photocatalytic dye degradation revealed anions, viz. nitrate, sulphate, oxalate and formate, which are released due to mineralization of dye solution by photocatalytic process. The performance of photocatalytic dye degradation was unchanged for 5 repetitive catalytic cycles and hence it was concluded that TPPO capped CuO nanoparticles offer excellent photocatalytic dye degradation ability when suitable electron capturing agents like potassium persulphate is used in tandem.

Key word: CuO nanoparticles, Photocatalytic dye degradation, Electron acceptor, Reactive oxygen species, Redox potential

1. Introduction

Increase in the usage of dyes in wide range of industries and their unregulated waste discharge in main stream aquatic system has led to severe impact on environment and human health [1, 2]. Dye contaminated colored water could reduce penetration of sunlight and subsequently hinder photosynthesis process in aquatic plants and eventually affect the ecosystem. This has prompted towards developing technologies for efficient dye removal from wastewater. Broadly, dye removal are based on adsorption and photocatalytic processes. In the case of adsorption, the dye transferred from one domain to another i.e., from aquatic medium to an adsorbent and therefore the toxicity effect of dye to the environment is not eliminated. For this reason degradation of dye is a preferred option for such remediation. Most industrial dyes are of complex structure

containing one or more azo (-N=N-) chromogenic groups which are stable against conventional methods of degradation [3, 4]. To a large extent advanced oxidation processes (AOP) based on Fenton's chemistry is successful for degradation of various types of dyes [5]. However, this method suffers from disadvantages e.g., the production of a substantial amount of $\text{Fe}(\text{OH})_3$ precipitate and additional water pollution caused by the homogeneous catalyst that added as an iron salt, cannot be retained in the process [6]. Lately, semiconductor type metal oxide nanoparticles (NPs) have evolved as an alternate class of photocatalyst for waste water treatment [7-11]. They are categorized as heterogeneous photocatalyst and hence can be re-used, which is an advantage over using ozone or chlorine as agents of advanced oxidation process.

The photocatalytic activity of metal oxides nanoparticles will depend on the ability of inhibiting electron-hole recombination. This essentially imply availability of the photoexcited electrons and holes to react with O_2 and H_2O molecules to form highly reactive oxygen species (ROS) e.g., singlet oxygen, superoxide radicals, hydroxide radicals [12, 13]. The conduction band electrons can reduce molecular oxygen to form highly reactive $\text{O}_2^{\cdot-}$ species. On the other hand, holes tend to oxidize H_2O to $\cdot\text{OH}$ radicals. However the feasibility of the ROS generation in the above scheme would depend on the energy levels of valence and conduction band electron of the metal oxide and the respective redox couples involved in the ROS production reaction. The electron-hole recombination can also be restricted by introducing an electron acceptor for extracting conduction band electrons [14]. The band gap of the metal oxides is an important parameter that quantifies harvesting of solar energy for photocatalytic process. Since band gap is inversely related to size of the photocatalyst nanoparticles [15], one can tune the band gap via tailor made size specific synthesis of the photocatalyst for optimum functioning by selecting suitable energy in the solar spectrum. In addition, the reduction in the sizes of the photocatalysts to nanoscale dimensions has an advantage over their bulk counterpart with respect to enhanced

photoabsorption owing to large surface area. The photocatalytic activity depends on the availability of reactive sites and charge diffusion length. Reduction in the sizes of the photocatalyst could potentially increase the interfacial charge transfer and decrease charge diffusion length, which minimizes volume charge recombination and promote photocatalytic activity of semiconductor nanoparticles [16]. Compared to the bulk CuO whose band gap is 1.2 eV, the CuO NPs of sizes ranging between 6 nm and 28.9 nm are reported with larger band gaps (1.3 eV – 2.1 eV) [17]. The CuO NPs with band gap greater than 2 eV can be considered to be suitable as it shifts the absorption of light from NIR region for bulk CuO to visible region in CuO nanoparticles. The reduction in the particle size not only increases the band gap but also results in increase in the surface area which is suitable for enhanced photoreaction. Though CuO NPs are extensively investigated for its applications in solar energy cells, electronics, gas sensors, biosensors, magnetic storage media, optical switch and batteries [18] but it is not widely studied as an efficient photocatalyst for dye degradation. It may be commented here that the photoexcited electrons and holes in the CuO NPs are not effectively separated to avoid recombination of excitons, which is a necessary condition for photocatalytic process. However, nanocomposites of CuO NPs prepared with ZnO, TiO₂, SnO₂ etc as co-catalysts are reported to exhibit excellent dye degradation [19-22]. The necessity of co-catalyst is attributed to favorable band structures of CuO and ZnO or TiO₂ for charge transfer and inhibition of excitonic recombination [23-26]. However, it is discussed in these studies that 100% photocatalytic degradation by the composites was not achievable due to the accumulation of electron-hole which favours recombination. In addition improper contact of CuO and other metal oxides in composites is also cited as cause for allowing recombination of electrons and holes. In this regard, a solid (photocatalyst)-liquid (electron acceptor) could be considered as a better approach for effective hindering of electron-hole recombination and consequently achieving better photocatalytic dye degradation.

Here we demonstrate the photocatalytic activity of CuO NPs in presence of electron acceptors as photocatalyst for degradation of complex azo-dye. We chose acid orange – 74 as an industrial test dye which contains chromium ions bound to azo group that offers stability to the dye structure and literature on its photocatalytic degradation is not common [27]. The CuO nanoparticles were prepared by controlled precipitation technique using triphenylphosphine oxide as a capping agent as a stabilizing agent. The dye degradation was studied by spiking with H₂O₂ and potassium persulphate as co-catalysts which are good electron acceptors. The mechanism of dye degradation has been established using theoretical calculation based on redox potentials of the co-catalyst which facilitated electron transfer process favorable for oxidative dye degradation.

2. Results and Discussion

2.1. Characterization of CuO nanoparticles

The XRD patterns of TPPO capped CuO NPs exhibited Bragg reflections at (111), (002), (200), (20 $\bar{2}$), (020), (202), (11 $\bar{3}$), (31 $\bar{1}$) and (220) planes (Fig.1), confirmed the synthesis of monoclinic structure of CuO (JCPDS No. 48-1548). The average crystallite size of the CuO NPs was determined to 7.5 ± 1.4 nm using Debye-Scherrer equation. The TEM image of CuO NPs revealed formation of spherical shaped particles of average size 8 nm (Fig. 2a), and the results are consistent with the crystallite size measured from XRD. The selected area electron diffraction (SAED) measurements of respective nanoparticles revealed circular rings attributable to their polycrystalline nature (Fig. 2b). The crystalline nature of the CuO NPs was further supplemented from the high resolution TEM image (HRTEM), which revealed lattice fringes and the difference between the two adjacent planes was determined to be 0.254 nm (Fig. 2c). Our result is consistent with the lattice constant of standard CuO in (002) plane [28]. The FESEM

measurements also revealed formation of spherical shaped CuO nanoparticles (Supplementary Fig. S1a). Corresponding EDX spectra revealed the characteristic X-ray peaks of Cu and O (Supplementary Fig. S1b), which confirmed the composition of these nanoparticles.

The band structure of the CuO nanoparticles was determined from diffused reflectance spectroscopic study, given in Fig. 3. The reflectance data was converted to absorption mode according to the Kubelka-Munk (K-M) theory [29]. The band gap of the samples was estimated from the Tauc's plot, using the Tauc expression [30]:

$$(\alpha h\nu)^{1/n} = A(h\nu - E_g)$$

where α , $h\nu$, A and E_g are the absorption coefficient, incident light frequency, proportionality constant and band gap, respectively. The value of exponent ' n ' determines the nature of electronic transition; e.g., $n = 1/2$ refers to direct transition, and $n = 2$ refers to indirect transition. Assuming direct transition for CuO nanoparticles, the linear region of the Tauc plot $(\alpha h\nu)^2$ against $h\nu$ was extrapolated to $(\alpha h\nu)^2 = 0$, which corresponded to the band gap energy of the material as 2.29 eV. The measured band gap was larger than that of the bulk CuO (1.2 eV). The increase in the band gap is attributable to the decrease in the particle size of the as-synthesized CuO nanoparticles, which is complemented with the TEM results. The effect of reduced particle size was reflected from larger BET specific surface area of 105.82 m²/g. Notably, the measured surface area of CuO nanoparticles was significantly higher than those reported for CuO nanoparticles synthesized by other methods [31-33]. Furthermore, the as synthesized CuO NPs exhibited high zeta potential ($\zeta = +30$ mV) at neutral pH (i.e. working condition for the dye degradation). This indicated that CuO NPs were well dispersed in aqueous medium which is suitable for photocatalytic activity. From the above results it may be summarized that the synthesis of large surface area of the photocatalyst (i.e., CuO NPs) is favourable for absorption of significant amount of photons for generating photoexcited electron-hole pairs. Further

enhanced band gap could facilitate absorption of photons in the visible region and hinder electron-hole recombination to favour visible light induced photocatalytic activity.

2.2 Photocatalytic dye degradation

Dye removal by a photocatalyst is often a combination of adsorption and photocatalytic process. The CuO NPs were equilibrated with dye solution in dark condition to account for any adsorption phenomenon. The results of dye adsorption on the CuO nanoparticles as photocatalyst performed in dark condition are given in Fig. 4a, which demonstrated increase in the % adsorption with the increase in the concentration of photocatalyst. In Fig. 4b, a plot of adsorption capacity (q_t) Vs time revealed that the equilibrium condition was achieved in 40 min for the batches of dye solutions treated with higher concentrations of photocatalyst (1.125 mg/mL and 1.50 mg/mL). However, equilibrium condition for the batches treated with 0.375 mg/mL photocatalyst was at 60 min where more than 90% adsorption was completed. After attaining equilibration in dark, all the batches of the dye solution treated with respective concentrations of photocatalysts were exposed to sunlight and the kinetics of the photocatalytic degradation studied in view of Langmuir-Hinshelwood model given as [34,35]:

$$\ln(C_0/C) = kt,$$

where ' C_0 ' is the initial concentration of the dye solution, ' C ' is the dye concentration at time ' t ' and ' k ' is the pseudo-first order rate constant.

It may be remarked here that there was no change in the concentration of the dye solution after 180 min sunlight exposure for the batches treated with 1.115 mg/mL and 1.500 mg/mL photocatalyst, respectively. The batch treated with 0.375 mg/mL photocatalyst, which exhibited 53% dye removal in dark condition by adsorption process, exhibited further 15% lowering of the concentration of the dye solution when exposed to sunlight for 180 min (Fig. 5a). The negative

control batch comprising of dye solution without photocatalysts under the sunlight exposure did not exhibit any change in the concentration of dye solution in 180 min. This indicated that the dye solution is stable under sunlight exposure. From these results, it may be inferred that the CuO nanoparticles exhibited weak photocatalytic property towards degradation of azo dyes. Contrastingly, 98% dye degradation was achieved in 180 min under sunlight exposure for the batches of dye solution treated with 0.375 mg/mL CuO NPs, when 400 μ L of H₂O₂ (30 % v/v) was spiked in the dye solution (Fig. 5a). The rate constant (k) for the dye degradation was derived as 0.0194 min⁻¹. Our results were consistent with the degradation of non-azo dye by CuO + H₂O₂ system [36,37]. Since H₂O₂ tends to produce hydroxyl radicals when exposed to sunlight, so it was necessary to assess whether the observed dye degradation in our study was primarily due to only H₂O₂ effect. The negative control experiment involving AO-74 dye solution spiked with same concentration of H₂O₂ but without treating with photocatalyst (i.e., CuO nanoparticles) under sunlight revealed much lesser dye degradation efficiency (40 %). It was therefore deduced that CuO nanoparticles had a role in achieving higher (98%) degradation of AO-74 dye solution using H₂O₂ as a co-catalyst. Notably, maximum dye degradation (99%) was achieved in 180 min under sunlight exposure when 5 mM potassium persulphate (K₂S₂O₈) was used as a co-catalyst for electron scavenging mechanism (Fig. 5b). The rate constant was calculated to be 0.0231 min⁻¹ which is greater than that of H₂O₂ treated batch. Further, unlike the case of hydrogen peroxide, the negative control experiment for the batch treated with K₂S₂O₈ did not exhibit any dye degradation (Fig. 5b). In the negative control experiment the dye solution was not treated with the photocatalyst (CuO NPs) but spiked with same concentration of K₂S₂O₈. This implied that K₂S₂O₈ alone cannot cause dye degradation under the sunlight exposure. Therefore it may be stressed here that photoexcitation of CuO NPs has a major role for accomplishing such high (99%) dye degradation, where S₂O₈²⁻ acted as co-catalyst.

2.3. Mechanism of photocatalytic degradation

2.3.1 Energy structure and hydroxyl radical production

The general mechanism of dye degradation by a metal oxide photocatalyst is based on oxidation processes carried out by the reactive oxygen species, e.g., hydroxyl radicals, superoxide anions and singlet oxygen species that are generated in the reaction medium [38]. It is well known that upon absorption of light with energy equal to or greater than the band gap of the metal oxide photocatalyst, results in the transition of photoexcited electrons to the conduction band while holes remain in the valence band. These excited electrons and holes could either (a) recombine and produce an intense fluorescence emission, or (b) find a pathway to the surface of the materials and interact with oxygen and water molecules to form various reactive oxygen species [39]. The production of a specific type of ROS, e.g., $\cdot\text{OH}$, $^1\text{O}_2$, or $\text{O}_2^{\cdot-}$ by metal oxide photocatalysts would however depend on electronic structure and the redox potentials (E_H) of the different ROS generation reactions. The electronic structure of metal-oxide nanoparticles is characterized by the band gap (E_g) corresponding to energy interval between the valence band (E_{VB}) and the conduction band (E_{CB}), each comprises of a high density of states. The conduction band edge minima (E_{CB}) and valence band maxima (E_{VB}) of the semiconductor photocatalysts could be empirically calculated using the following expressions [40]:

$E_{CB} = \chi(A_aB_b) - \frac{1}{2}E_g + E_o$; and $E_{VB} = E_{CB} + E_g$; where, E_g is the band gap of the semiconductor, E_{CB} is the potential of the conduction band, E_{VB} is the valence band potential, E_o is the scale factor taken as -4.50 eV, i.e., the energy of free electrons on the normal hydrogen electrode (NHE scale). The parameter $\chi(A_aB_b)$ corresponds to the absolute electronegativity of a semiconductor material type A_aB_b , which is calculated as the geometric mean of the electronegativity of the constituent atoms. In our calculation, the electronegativity values for Cu and O were taken as 4.48 eV, and 7.54 eV respectively [41].

However the band edges are dependent on the pH of the medium. The pH dependent conduction band edge E_C and valance band edge E_V energies were calculated by incorporating pH in the Nerstian relation discussed below [42]:

$$E_{C, pH} = E_{CB} + 0.059 \times (PZZP - pH)$$

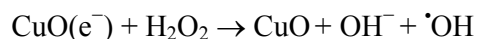
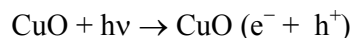
$$E_{V, pH} = E_{VB} + 0.059 \times (PZZP - pH)$$

where PZZP is the point of zero zeta potential of TPPO capped CuO NPs. The PZZP value (pH = 9.20) was calculated from the series of zeta potential measurements against different pH of the medium ranging between pH 5 and pH 12 (Supplementary Fig. S2). The pH corrected E_C and E_V of TPPO capped CuO at pH 7 were determined to be 0.29 eV and 2.59 eV, respectively. These values are comparable with those reported for smaller sized CuO NPs [37, 43].

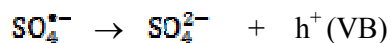
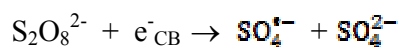
Notably, the calculated E_C value of CuO is greater than the E_H (redox potential) of $O_2/O_2^{\cdot-}$ (-0.2 eV Vs NHE [44]). So the potential of the E_C was less than that of $O_2/O_2^{\cdot-}$, due to which the photo-excited electrons in the conduction band of CuO could not reduce molecular oxygen to $O_2^{\cdot-}$. On the other hand, the E_H for the hole induced $H_2O/^{\cdot}OH$ generation is approximately 2.2 eV with respect to NHE, which is less than the calculated E_V value of CuO. This implied that the holes generated due to absorption of sunlight by CuO NPs could potentially oxidize H_2O into $^{\cdot}OH$ radicals. However existence of free holes might not be available as the photoexcited electrons would tend to recombine with holes. This is evident from the observation of strong fluorescence intensity exhibited by CuO nanoparticles at $\lambda = 365$ nm and 469 nm when excited at 300 nm (Supplementary Fig. S3). Therefore the ROS generation by CuO is not favourable and subsequently reflected poor photocatalytic dye degradation efficiency as observed in our experiments on degradation of AO-74 azo dye.

However, a striking improvement in the photocatalytic dye degradation was observed in the presence of electron acceptors like H_2O_2 and $K_2S_2O_8$. This is attributable to generation of

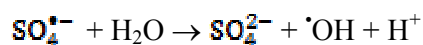
hydroxyl radicals owing to thermodynamically favoured reduction of H_2O_2 by the conduction band electrons as the E_{CB} of CuO is less than the E_{H} of $\text{H}_2\text{O}_2/\cdot\text{OH}$ (which is given as 0.87 eV in the NHE) [45]. The possible reactions are given below:



In the case of spiking with potassium persulphate, the highly reactive $\text{SO}_4^{\cdot-}$ species are formed due to reduction of $\text{S}_2\text{O}_8^{2-}$ by conduction band electrons owing to its high redox potential (2.01 eV). The reduction of $\text{S}_2\text{O}_8^{2-}$ is considered as a two-step process given below [46]:



These holes interact with H_2O to produce highly reactive $\cdot\text{OH}$ (E_{H} of $\text{H}_2\text{O}/\cdot\text{OH}$ is 2.2 eV), which are responsible for the observed dye degradation. The feasibility of reduction of $\text{S}_2\text{O}_8^{2-}$ to sulphate radical is attributed to high redox potential of $\text{S}_2\text{O}_8^{2-} / \text{SO}_4^{\cdot-}$ (2.01 eV) [45]. Overall, the sulphate radical ($\text{SO}_4^{\cdot-}$) interacts with water in the reaction medium to produce highly oxidative hydroxyl radical as shown below [47]:



According to the proposed mechanism for the photocatalytic degradation, it is apparent that the electron acceptor e.g., $\text{K}_2\text{S}_2\text{O}_8$ molecules are adsorbed on the surface of CuO nanoparticles for accepting the photo-excited electrons. In this regard the TPPO capping assumedly enhanced the adsorption of electron acceptor like $\text{K}_2\text{S}_2\text{O}_8$ via electrostatic interaction between $\text{S}_2\text{O}_8^{2-}$ and the positive surface charge on TPPO capped CuO NPs for production of sulphate radical followed by generation of hydroxyl radicals as described above.

The phenomenon of ROS generation in general and hydroxyl radicals in particular, in our photocatalytic studies was established by studying the photocatalytic dye (AO-74) degradation in

the presence of ROS scavengers in the reaction medium. Chloroform was chosen as $O_2^{\cdot-}$ scavenger while isopropyl alcohol was used as $\cdot OH$ scavenger [48]. Isopropyl alcohol containing α -hydrogen is highly reactive to $\cdot OH$ radical and poorly reactive to $O_2^{\cdot-}$ [49]. The batches of AO-74 solution treated with CuO nanoparticles spiked with H_2O_2 and isopropyl alcohol revealed reduced rate of dye degradation from $k = 0.022 \text{ min}^{-1}$ to $k = 0.010 \text{ min}^{-1}$, while the batch treated with chloroform did not show any reduction in dye degradation rate (Fig. 6a). This indicated that isopropyl alcohol could scavenge the $\cdot OH$ radicals generated in the reaction medium for which the dye degradation rate was reduced. On the other hand, the batch treated with chloroform did not reveal any change in the rate of degradation as $O_2^{\cdot-}$ species were not likely to be generated. Similarly, the rate of degradation of the batch of the AO-74 dye solution spiked with $K_2S_2O_8$ reduced from $k = 0.022 \text{ min}^{-1}$ to $k = 0.0062 \text{ min}^{-1}$ when isopropyl alcohol was added as $\cdot OH$ scavenger (Fig. 6b). Generation of $O_2^{\cdot-}$ radicals in the reaction medium was least probable as the batch of dye solution treated with chloroform as $O_2^{\cdot-}$ scavenger, did not exhibit any reduction rate.

Our studies using ROS specific scavengers elucidated that $\cdot OH$ is the dominant reactive oxygen species during photocatalytic dye degradation process of CuO nanoparticles cocktailed with $K_2S_2O_8$ or with H_2O_2 as co-catalyst. These experimental results are consistent with our theoretical analysis of charge transportation using the energy levels of the band structure of CuO and the redox potentials of the relevant ROS reactions.

2.3.2 Anionic degradation product analysis by Ion Chromatography

The evidence of dye degradation was further confirmed from measuring the anionic products in the dye solution that were released during photocatalytic dye degradation process. Ion chromatograph of the dye solution after treating with CuO NPs and H_2O_2 revealed peaks

corresponding to nitrate, sulphate, oxalate and formate anions (Fig. 7). These anionic species are reported to be released due to mineralization of dye solution by photocatalytic process for dye containing azo groups and SO_3H functional groups. The evolution of SO_4^{2-} indicates the mineralization of $-\text{SO}_3$ containing aromatic intermediates [50]. The nitrogen in the dye molecule is likely to be transformed into others nitrogen species such as NO_3^- or gas N_2 and/or NH_3 during photodegradation process [51]. The appearance of oxalates and formates in the ion chromatograph is attributable to formation of oxalic acid and formic acid, which are some of the well known by-products of complete mineralisation of azo-dye like acid orange 7 [52]. Though carboxylic acids are known to be the ultimate by-products of aromatic ring opening reactions during complete mineralization of azo dyes [53], but it could not be detected in our ion chromatography study as it might have interfered with sodium carbonate and sodium bicarbonate solutions were used as the eluents.

2.4. Photostability and re-usability of CuO nanoparticles

In order to evaluate the stability and re-usability of the five cycles of degradation process (i.e., equilibration in dark followed by sunlight exposure) were repeated in presence of H_2O_2 as a co-catalyst. In all the five cycles, $\sim 98\%$ degradation of AO-74 dye was achieved in 180 min of sunlight exposure and their respective rate constants (k) were of similar order (Fig. 8). This indicates that there was no loss of photocatalytic activity of TPPO capped CuO NPs.

3. Experimental

3.1. Chemicals

Copper acetate ($\text{Cu}(\text{CH}_3\text{COO})_2$, $> 98\%$), acetic acid (CH_3COOH , 99.5%), sodium hydroxide (NaOH , $> 98\%$), hydrogen peroxide (30% v/v), potassium persulphate ($\text{K}_2\text{S}_2\text{O}_8$, 99%) and

ethanol (> 99 %) were procured from HiMedia Pvt. Ltd., India. Triphenylphosphine oxide (> 98 %) and acid orange 74 (60 %) dye were procured from Sigma Aldrich, GmbH, Germany. All reagents and precursors used in this study were of analytical grade and were used without further purification.

3.2. Synthesis of CuO nanoparticles

The batches of TPPO capped CuO NPs were prepared by mixing 150 mL of 0.02 M of copper acetate aqueous solution with 0.1 g of TPPO and 2 mL acetic acid in a round-bottomed flask and refluxed at 100 °C for 1 h. Then 1.0 M NaOH was added to the solution until a black colored CuO precipitate was produced at pH 7-8. The precipitate was centrifuged at room temperature and washed with deionized water (Millipore) and ethanol, and eventually dried at 60 °C overnight in a temperature controlled oven. The capping agent TPPO stabilized the CuO NPs and rendered surface affinity for reactants, e.g. dye molecules. This phenomenon might facilitate adsorption of oppositely charged target material by electrostatic interaction. Consequently, the residence time of the target molecules on the surface of the photocatalyst would be more and subsequent photocatalytic efficiency might be enhanced.

3.3. Characterization of capped CuO nanoparticles

The X-ray powder diffraction (XRD) patterns were recorded on Bruker ARS D8 Advance diffractometer using graphite monochromatized Cu K α radiation ($\lambda = 1.5406 \text{ \AA}$) in a 2θ range from 20° to 80° at a scanning rate of 2°/min. Transmission electron microscopy (TEM) images were recorded with FEI Technai-G2 microscope, operated at an acceleration voltage of 200 kV. Scanning electron microscopy (SEM) images were recorded with Zeiss FE-SEM, Ultra plus55, operating at an accelerating voltage of 20 kV. The elemental composition of the nanoparticles

was determined by energy dispersive X-ray spectrometer (EDX) attached with SEM. The Brunauer Emmett and Teller (BET) specific surface area of the nanoparticles were measured by Quantachrome Nova 2200 analyser at liquid nitrogen temperature using nitrogen adsorption-desorption method. The UV-visible absorption spectroscopy studies were performed in the wavelength range of 200–800 nm using Shimadzu, UV-1800. The emission spectra were recorded using Shimadzu (RF-5301 PC) fluorescence spectrophotometer at an excitation wavelength (λ_{ex}) of 300 nm.

3.4. Zeta potential measurement

The zeta potential of the TPPO capped CuO nanoparticles were measured at different pH (i.e., pH = 5, 7, 8, 9, 10, 11 and 12) using Malvern Zeta Sizer Nano ZS90. The pH of the solutions was adjusted by adding dilute hydrochloric acid (0.1 M) or sodium hydroxide (0.1 M). The experiments were carried out by dispersing 5 mg of solid catalyst in 50 mL aqueous solutions and sonicated for 10 min.

3.5. Equilibration of dye with photocatalyst in dark condition

Batches of 40 mL AO-74 dye solution of initial concentrations 0.075 mg/mL were treated with 0.375 mg/mL, 0.75 mg/mL, 1.125 mg/mL and 1.50 mg/mL of the TPPO capped CuO NPs, respectively in dark condition under slow stirring for 150 min at room temperature. 1 mL aliquot was withdrawn and centrifuged at 15000 rpm for 5 min at predetermined time. The dye concentration in supernatant was determined by measuring the absorbance using UV-Visible spectrophotometer. The % decolourization of dye in supernatant is a measure of the amount of AO-74 dye adsorbed on the catalyst surface at any time determined by:

$$\% \text{ decolorization} = \frac{C_o - C_t}{C_o} \times 100$$

C_o = initial concentration of AO-74 dye (mg/L); C_t = concentration of AO-74 dye at time (t)

The de-colorization efficiency of acid orange-74 increased with the concentration of TPPO capped CuO nanoparticles. The adsorption capacity of catalysts was determined as follows:

$$q_t = (C_o - C_t) \times \frac{V}{w}$$

where C_o and C_t are dye concentrations (mg/mL) at time 0 and t, respectively, V is the volume of the solution (mL), and m is weight of the catalysts. The concentration of the CuO photocatalyst was chosen as 0.375 mg/mL for systematic photocatalytic studies.

3.6. Photocatalytic degradation of Acid Orange 74 dye

After equilibrating the dye solution with TPPO capped photocatalyst for 60 min in dark condition, the reaction mixture containing 0.375 mg/mL photocatalyst was exposed to natural sunlight (degradation experiments were carried out at IIT Roorkee (29°51'N; 77°53'E) in the month of November, 2014). Further sunlight induced photocatalytic dye degradation studies were conducted by spiking 400 μ L of 30% (v/v) H_2O_2 to the reaction medium after equilibrating in dark condition described above. Similarly, photocatalytic dye degradation by TPPO capped CuO nanoparticles were studied by adding 1 mM, 3 mM and 5 mM potassium persulphate in to the reaction medium. To differentiate between the photocatalysis and the photolysis of AO 74, control experiment under light exposure was carried in the absence of NPs as catalyst. In all the cases, the kinetics of decolorization of the dye was studied by withdrawing 1 mL aliquot dye solution at specific time interval. The dye concentration in the supernatant fraction was measured after centrifuging at 15,000 rpm at 25 °C for 5 min using Beckman Coulter Allegra™ X-22R.

3.7 Analysis of degradation products by ion chromatography

Inorganic anions released during the photodegradation of AO-74 dye were determined by ion chromatography using Ion Chromatograph (Mettrohm 882 Compact IC plus). The anion separation study was conducted using Metrosep Supp 5-150 column where 5 mM Sodium carbonate and 0.5 mM Sodium bicarbonate as eluent with 0.7 mL/min flow rate. Standard solutions of formate, oxalate, nitrate and sulphate were prepared for identifying the anionic species produced in the reaction mixture after dye degradation process.

3.8. Scavenging of reactive oxygen species (ROS)

To detect the active reactive oxygen species responsible for photodegradation, different scavengers were added to the dye solution along with catalysts and oxidising agent (H_2O_2 and $\text{K}_2\text{S}_2\text{O}_8$). The dye solution (0.075 mg/ mL) is treated with 0.375 mg/mL catalysts and 400 μL H_2O_2 and was stirred in dark for 1 h. Then isopropyl alcohol (IPA, 1mM) and chloroform (1mM) was added to the respective batches. These batches were then exposed to sunlight for photodegradation studies. Same experiment has been repeated for studying scavenging of ROS generated by CuO and 5 mM $\text{K}_2\text{S}_2\text{O}_8$ system.

3.9. Photostability and reusability of CuO nanoparticles

The stability of CuO NPs against photocorrosion and reusability of the catalyst was investigated by conducting five degradation cycles with same catalyst. For this, 0.375 mg/mL CuO NPs were taken in 0.075 mg/mL acid orange dye (AO74) solution and the photocatalytic degradation studies were performed. After each cycle, the catalyst was separated by centrifuging and further used for next cycle without washing. For each cycle studies, the dye catalyst suspension was

subjected to 60 min dark stirring followed by addition of H₂O₂ and then photocatalytic degradation in sunlight.

4. Conclusions

The photocatalytic degradation efficiency of azo dye (acid orange 74) by CuO nanoparticles was enhanced to 99 % by inhibiting photoexcited electron-hole recombination when suitable electron acceptors are used in the reaction medium. Compared to H₂O₂, the rate of dye degradation was higher for the batch treated with K₂S₂O₈ which is attributed to formation of highly oxidizing $\text{SO}_4^{\cdot-}$ and $\cdot\text{OH}$ radicals. Adsorption of electron acceptors like K₂S₂O₈ on the surface of TPPO capped CuO NPs was considered to be favourable for transfer of photoexcited electrons and holes from the conduction band and valence band of CuO NPs respectively and subsequent production of highly reactive $\text{SO}_4^{\cdot-}$ and $\cdot\text{OH}$ free radicals was proposed to be the key mechanism for photocatalytic dye degradation of acid orange 74. Specific ROS scavenger test by isopropyl alcohol indicated generation of hydroxyl radicals as major species in the dye degradation. The mineralization of the dye was confirmed by determining the release of inorganic anions *e.g.*, sulphate, nitrate, acetate and formate by ion chromatography.

Acknowledgment

Aarti Sharma is thankful to Ministry of Human Resource Development (MHRD), Govt of India for awarding Senior Research Fellowship. Authors also thank Institute Instrumentation Centre of IIT Roorkee for the instrumental facilities.

Reference

1. H. Kusic, N. Koprivanac, A.L. Bozic. *J. Photochem. Photobiol. A*, 2013, 252, 131-144.
2. L. Pereira, M. Alves. *Environmental Protection Strategies for Sustainable Development* Eds. A. Malik, E. Grohmann, Springer, New York, 2012, Vol. 14, Ch 4, pp 111-162.
3. M. R. Hoffmann, S. T. Martin, W. Choi, D. W. Bahnemann. *Chem. Rev.* 1995, 95, 69-96.
4. A. C. Robles, E. Martinez, I. R. Alcantar, C. Frontana, L.G. Gutierrez. *Bioresource Technol.* 2013, 127, 37-43.
5. P. V. Nidheesh, R. Gandhimathi, S. Velmathi, N. S. Sanjini. *RSC Adv.* 2014, 4, 5698.
6. S. Chou, C. Huang, Y. H. Huang. *Chemosphere*, 1999, 39, 1997-2006.
7. H. S. Rai, M. S. Bhattacharyya, J. Singh, T. K. Bansal, P. Vats, U. C. Banerjee. *Crit. Rev. Env. Sci. Technol.* 2005, 35, 219–238.
8. M. A. Rauf, S. S. Ashraf. *J. Hazard. Mater.* 2009, 166, 6-16.
9. K. Rajeshwar, M. E. Osugi, W. Chanmanee, C.R. Chenthamarakshan, M.V.B. Zaroni, P. Kajitvichyanukul, R. Krishnan-Ayer. *J. Photochem. Photobiol.C: Photochem. Rev.* 2008, 9, 171–192.
10. D. Zhang, G. Li, J. C. Yu. *J. Mater. Chem.* 2010, 20, 4529–4536.
11. A. D. Paola, E. García-López, G. Marci, L. Palmisano. *J. Hazard. Mater.* 2012, 211, 3–29.
12. K. V. Baiju, S. Shukla, K. S. Sandhya, J. James, K. G. K. Warriar. *J. Phys. Chem. C*, 2007, 111, 7612–7622.
13. R.K. Dutta, N.B. Prasad, M.K. Gangishetty, A.V.R. Reddy, *Colloids. Surf. B.* 2012, 94, 143-150
14. A. L. Stroyuk, A. I. Kryukov, S. Ya. Kuchmii, V. D. Pokhodenko. *Theor. Exp. Chem.* 2005, 41, 207-228.
15. S. Baskoutas, A.F. Terzis, *J. Appl. Phys. Lett.* 2006, 99, 013708 – 013711.

16. S. Rehman, R. Ullah, A. M. Butt, N. D. Gohar. *J. Hazard. Mater.* 2009, 170, 560–569.
17. R. V. Kumar, R. Elgamiel, Y. Diamant, A. Gedanken. *Langmuir*, 2001, 17, 1406-1410.
18. Q. Zhang, K. Zhang, D. Xu, G. Yang, H. Huang, F. Nie, C. Liu, S. Yang. *Prog. Mat. Sci.* 2014, 60, 208–337.
19. B. Li, Y. Wang. *Superlattice. Microst.* 2010, 47, 5, 615–623.
20. S. Wei, Y. Chen, Y. Ma, Z. Shao. *J. Mol. Catal. A: Chem.* 2010, 331, 112–116.
21. H. Xia, H. Zhuang, T. Zhang, D. Xiao. *J. Environ. Sci.* 2007, 19, 1141–1145.
22. F. Zhang, Z. Cheng, L. Kang, L. Cui, W. Liu, G. Hou, H. Yang, X. Xu. *RSC Adv.* 2014, 4, 63520-63525.
23. B. Li, Y. Wang. *Superlattice Microst.* 2010, 47, 615–623.
24. G. Li, N. M. Dimitrijevic, L. Chen, T. Rajh, K. A. Gray. *J. Phys. Chem. C*, 2008, 112, 19040–19044.
25. J. Bandara, C. P. K. Udawatta, C. S. K. Rajapakse. *Photochem. Photobiol. Sci.* 2005, 4, 857-861.
26. R. Saravanan, S. Karthikeyan, V. K. Gupta, G. Sekaran, V. Narayanan, A. Stephen. *Mat. Sci. Eng. C-Biomim.* 2013, 33, 91–98.
27. A. El-Trass, H. El-Shamy, I. El-Mehasseb, M. El-Kemary. *Appl. Surf. Sci.* 2012, 258, 2997–3001.
28. Y. Liu, L. Zhong, Z. Peng, Y. Song, W. Chen. *J. Mater. Sci.* 2010, 45, 3791-3796.
29. G. Kortum. *Reflectance Spectroscopy*, Springer-Verlag, New York, 1969.
30. J. Tauc, R. Grigorovic, A. Vancu. *Phys. Status Solidi*, 1966, 15, 627-637.
31. M. Sahooia, S. Sabbaghi, R. Saboori. *Mater. Lett.* 2012, 81, 169–172.
32. K. V. Kumar, K. Porkodi, F. Rocha. *Catal. Commun.* 2008, 9, 82–84.
33. C. S. Turchi, D. F. Ollis. *J. Catal.* 1990, 122, 178-192.
34. H. Xu, G. Zhu, D. Zheng, C. Xi, X. Xu, X. Shen. *J. Colloid Interf. Sci.* 2012, 383, 75–81.

35. J. Li, F. Sun, K. Gu, T. Wu, W. Zhai, W. Li, S. Huang. *Appl. Catal. A*, 2011, 406, 51-58.
36. X. Liu, Z. Li, Q. Zhang, F. Li, T. Kong. *Mater. Lett.* 2012, 72, 49–52.
37. A. N. Ejhieh, M. K. Shamsabadi. *Chem. Eng. J.* 2013, 228, 631–641.
38. Y. Li, W. Zhang, J. Niu, Y. Chen. *ACS Nano*, 2012, 6, 5164–5173.
39. W. He, H. K. Kim, W. G. Wamer, D. Melka, J. H. Callahan, J. J. Yin. *J. Am. Chem. Soc.* 2014, 136, 750-757.
40. R. R Reddy, Y. N. Ahammed, K. R. Gopal, D. V. Raghuram. *Opt. Mater.* 1998, 10, 95–100.
41. R. G. Pearson. *Inorg. Chem.* 1988, 27, 734-740.
42. Y. Xu, M. A. A. Schoonen. *Am. Miner.* 2000, 85, 543–556.
43. F. P. Koffyberg. *J. Appl. Phys.* 1982, 53, 1173.
44. P. J. Wardman. *Phys. Chem. Ref. Data*, 1989, 18, 1637-1755.
45. J. J. Kelly, E. S. Kooij, D. Vanmaekelbergh. *Langmuir*, 1999, 15, 3666-3671.
46. C. Liang, C. J. Bruell, M. C. Marley, K. L. Sperry. *Chemosphere*, 2004, 55, 1213–1223.
47. A. V. Rupa, D. Manikandan, D. Divakar, T. Sivakumar. *J. Hazard. Mater.* 2007, 147, 906–913.
48. J. D. Laat, T. G. Le. *Environ. Sci. Technol.* 2005, 39, 1811–1818.
49. S. Hwang, S. G. Huling, S. Ko. *Chemosphere*, 2010, 78, 563–568.
50. S. Hammami, N. Bellakhal, N. Oturan, M. A. Oturan, M. Dachraoui. *Chemosphere*, 2008, 73, 678–684.
51. K. Vinodgopal, J. Peller. *Res. Chem. Intermediat.* 2003, 29, 307–316.
52. M. Styliidi, D. I. Kondarides, X. E. Verykios. *Appl. Catal. B - Environ.* 2004, 47, 189–201.
53. B. Boye, M. M Dieng, E. Brillas. *Environ. Sci. Technol.* 2002, 36, 3030–3035.

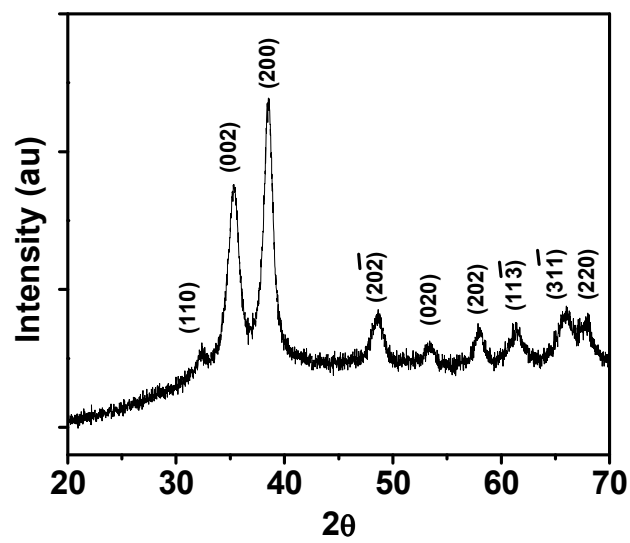


Fig. 1

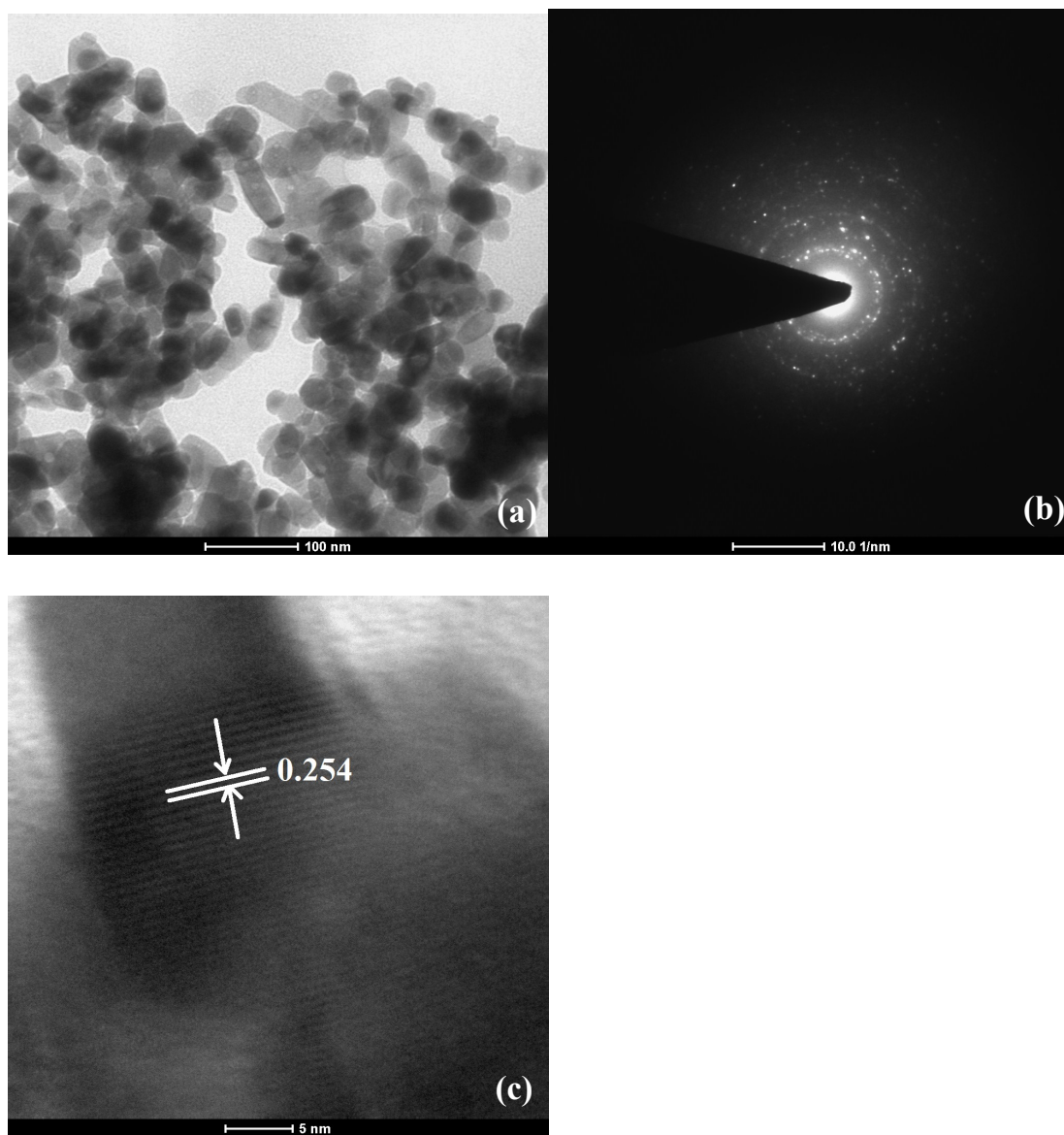


Fig. 2

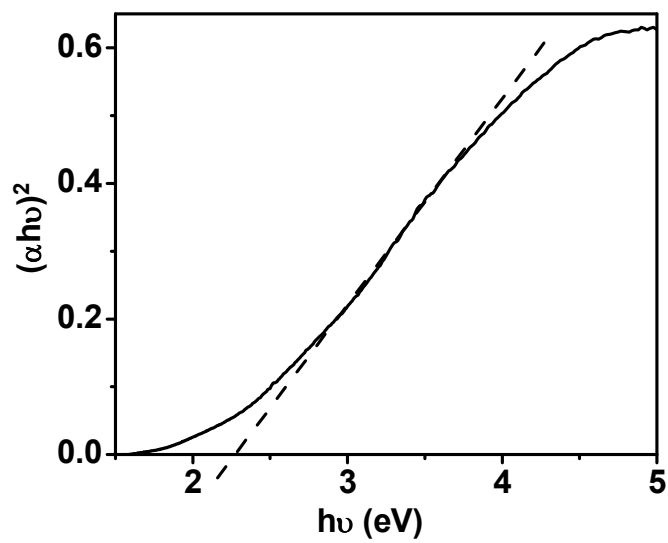


Fig. 3

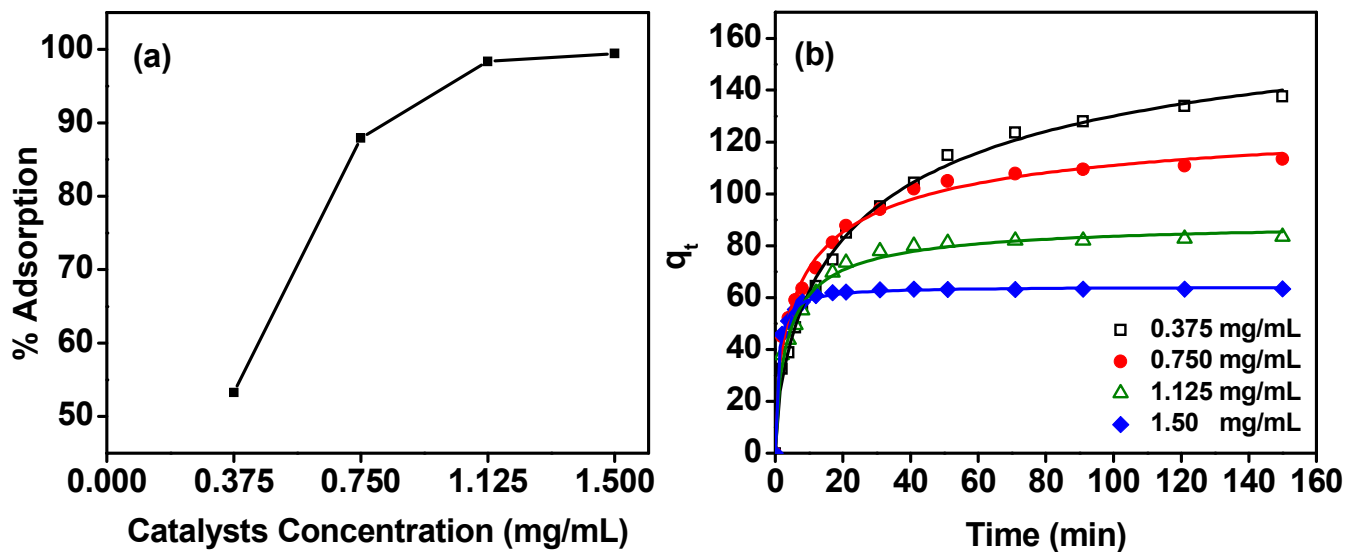


Fig. 4

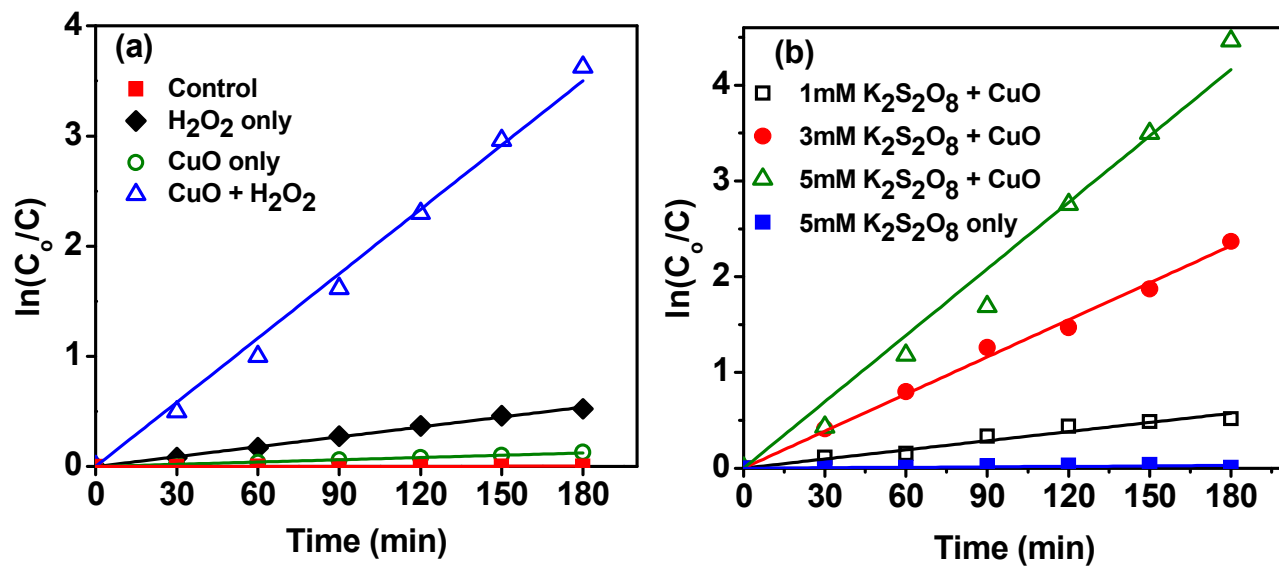


Fig. 5

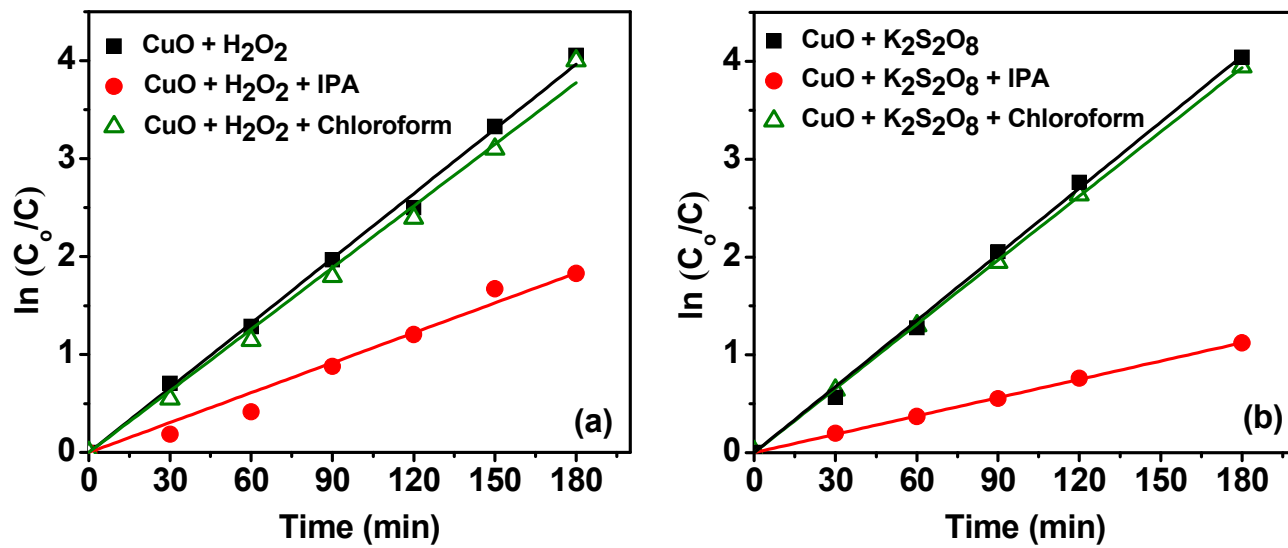


Fig.6

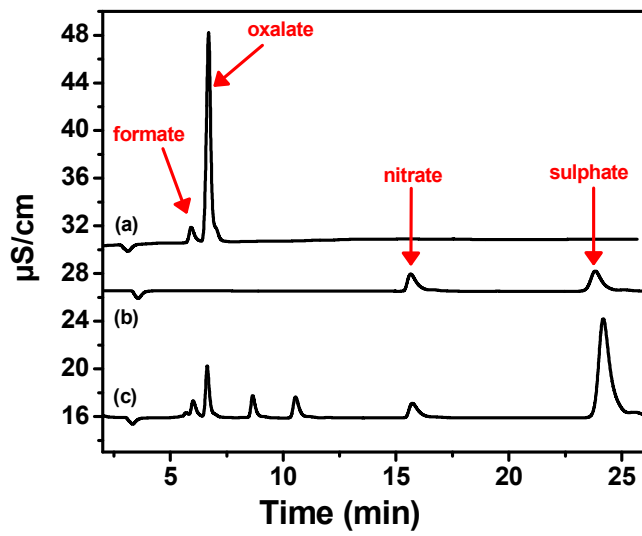


Fig. 7

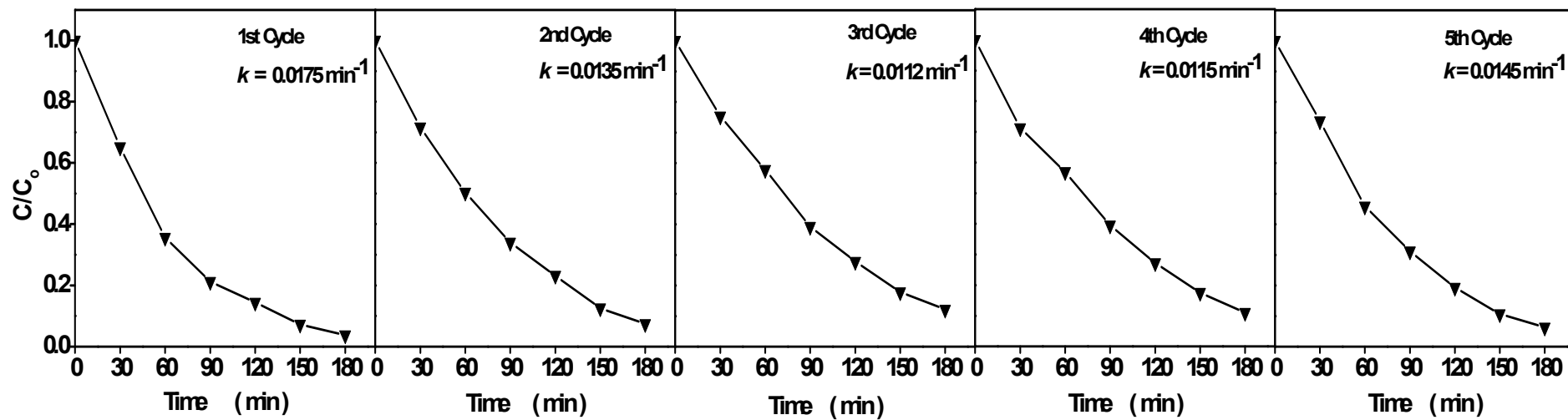


Fig. 8

FIGURE CAPTION

Fig. 1 X-ray diffraction pattern of 8 nm sized CuO NPs

Fig. 2(a) Transmission electron microscopy (TEM) of CuO NPs; (b) selected area electron diffraction (SAED) pattern of CuO NPs; (c) High resolution TEM (HRTEM) of CuO NPs revealing lattice fringes.

Fig. 3 Kubelka-Munk plot for the calculation of band gap of CuO NPs.

Fig. 4(a) The percentage adsorption of AO-74 dye on catalysts surface (b) The pseudo-second order kinetics model of AO-74 adsorption on CuO NPs;

Fig. 5 The plot of $\ln(C_0/C)$ as a function of time by CuO NPs (a) in the presence of H_2O_2 (b) in the presence of $K_2S_2O_8$ under sunlight.

Fig. 6 Effects of different scavengers on the degradation of AO 74 by CuO NPs in (a) presence of H_2O_2 (b) in presence of $K_2S_2O_8$ under sunlight.

Fig. 7 Ion chromatograph of mineralisation of dye (a) standard of nitrate and sulphate (b) standards of formate and oxalate (c) degraded product by CuO NPs

Fig. 8 Time profiles of AO-74 degradation for five successive cycles with CuO NPs in presence of H_2O_2 under sun-light irradiation.